Surface Reactivity of Pd Nanoparticles Supported on Polycrystalline Substrates As Compared to Thin Film Model Catalysts: Infrared Study of CO Adsorption

Serena Bertarione,[†] Domenica Scarano,*,[†] Adriano Zecchina,[†] Viktor Johánek,[‡] Jens Hoffmann,[‡] Swetlana Schauermann,[‡] Martin M. Frank,[‡,§] Jörg Libuda,[‡] Günther Rupprechter,[‡] and Hans-Joachim Freund[‡]

Dipartimento di Chimica Inorganica, Chimica Fisica e Chimica dei Materiali, Università di Torino, via P. Giuria 7, 10125 Torino, Italy, Consorzio INSTM, Via Benedetto Varchi n. 59, 50132 Firenze, Italy, Fritz-Haber-Institut der Max-Planck-Gesellschaft, Faradayweg 4-6, 14195 Berlin, Germany, and IBM T.J. Watson Research Center, P.O. Box 218, Yorktown Heights, New York 10598

To identify the nature and the local structure of the surface of supported catalyst nanoparticles, we have performed a detailed comparative study of CO adsorption on two categories of oxide-supported Palladium catalysts: (1) polycrystalline MgO and γ-Al$_2$O$_3$ supported Pd metal catalysts prepared by impregnation techniques and characterized by different degrees of regularity and perfection and (2) single-crystal based Pd model catalysts prepared under ultrahigh vacuum (UHV) conditions. The assignment of the CO vibrational frequencies to different types of sites on these systems has allowed a detailed structural characterization. For the Pd model catalyst, at low CO coverage, the infrared (IR) reflection absorption spectra closely resemble the expected behavior for terminations by a majority of (111) facets and a minority of (100) facets. The spectral features are indicative of defect sites such as particle steps and edges. Occupation of the defect sites can be affected by surface contaminations such as atomic carbon. Thus the CO spectra at high coverage can be used as both a structural and chemical probe under reaction conditions, provided that complementary information on the particle morphology is available. For the MgO and γ-Al$_2$O$_3$ supported Pd systems, two distinct narrow bands ($\nu \cong 2070$ and $\cong 1970$ cm^{-1}) have been assigned to linearly bonded and bridge-bonded CO species, on Pd (100)/(111) edges or facets, in agreement with the previous results obtained on model catalysts. The broad character of the 2070 cm^{-1} feature indicates the simultaneous presence of (100) and (111) faces, with edge and corner sites present at their intersection. The high intensity and the small half-width (fwhm) of the band at 1970 cm^{-1} on a Pd/MgO sample treated at high temperature, assigned to bridge-bonded CO species, suggests that the metal particles expose faces with a high level of regularity. Further spectroscopic features ($\nu \cong 1920-1800$ cm^{-1}), are ascribed to the presence of different types of 3-fold hollow sites on (111) faces.

1. Introduction

The atomic-level understanding of the processes in heterogeneous catalysis has received remarkable interest in recent years. Experimentally, such processes have become much more accessible by the development of model catalysts, constituted by metal particles deposited onto oxide single crystals cleaved in ultrahigh vacuum (UHV) [1−3] or onto ordered oxide films epitaxially grown on single crystalline metal surfaces.[4−14] As a matter of fact, utilizing powerful surface science techniques under UHV conditions has generated, in a controlled and reproducible way, model catalysts having different structures and morphology.

Historically, surface science work initially addressed the reactivity of metal single crystals with well-defined orientations under UHV conditions. This allowed us to identify active surface sites as well as relevant reaction intermediates, promoters and inhibitors.[15,16] Recently, the problem of the so-called "pressure gap" has been addressed as well by means of suitable high-pressure cells coupled to UHV chambers, where catalytic reactions at high pressures can be studied and surface composition and structure can be determined before and after reaction.[17−19]

These single-crystal investigations provided insight into many fundamental processes and allowed comparison with high surface area supported catalysts.[20−22] However, a complete understanding of catalytic reactivity cannot be achieved by utilizing metal single crystals alone, because the interaction between a metal and its support and particle size effects can alter the activity and selectivity of supported catalysts in a remarkable way. This can be due to changes in the average metal atom coordination number, in the morphology, and in the different nature of metal−support interaction as the fraction of metal atoms in direct contact with the substrate varies. One approach to overcome this so-called "materials gap" between the two domains is the preparation of model oxide supported metal catalysts in UHV. These systems are characterized by a complexity that is intermediate between single crystals and high surface area supported materials, allowing detailed studies on the electronic properties, adsorption behavior, and catalytic activity.[7−14]

---
* Corresponding author. Tel: +39 011 6707834. Fax: +39 011 6707855. E-mail address: domenica.scarano@unito.it.
† Università di Torino and Consorzio INSTM.
‡ Fritz-Haber-Institut der Max-Planck-Gesellschaft.
§ IBM T.J. Watson Research Center.

Although these investigations on ordered oxide films epitaxially grown on single crystal metal faces and on single crystal oxide surfaces only started recently, dispersed materials have received much more attention in the past because they are certainly representing some of the most important and widely employed classes of solids finding application in catalysis as true active phases or as supports of active phases (dispersed metals).[23] On the other hand, it is known that the complexity of the "real world" systems, like those represented by high surface area oxide supported metal catalysts, makes it difficult to obtain a detailed picture of their microscopic properties. However, in recent years, besides the recently available correlations between planar model supported catalysts and their analogous high surface area counterparts, it has been shown that well-defined polycrystalline oxide supported metal particles can been obtained; they can assume the morphology of very well defined polyhedra and consequently expose facets whose regularity and perfection are not fundamentally different from those encountered in particles deposited on single crystals.[24] As described before, the reactivity of these systems depends not only on the type of materials involved but also on the morphology and size of the metal particles. More specifically, on small metal clusters the presence of high energy adsorption sites increases, as evidenced by Fourier transform infrared spectroscopy (FTIR) studies of CO adsorbed on supported metal clusters Pd/MgO (100) [2]. This implies that the catalytic activity of nanoparticles may by critically controlled by their microscopic structure or by the presence of coadsorbed species.

The aim of these FTIR studies is to investigate the surface properties of MgO supported Pd crystallites through the adsorption of CO (this work) and CH_3OH.[25] We study Pd particles of different degrees of regularity and perfection in comparison with analogous thin film supported metal particles. In contrast to IR spectra of CO on $Pd/\gamma Al_2O_3$ polycrystalline systems, which reveal a high level of defectivity and disorder, the MgO support is preferred because (i) Pd/MgO is known to be an efficient catalysts for methanol synthesis from $H_2 + CO$ and (ii) the more regular structure of MgO crystallites of the support is expected to have influence on the morphology of the Pd microcrystals, favoring the growth of well-defined crystallites.

Adsorption of CO and CH_3OH on model systems are investigated, which consist of nanosized Pd particles supported on ordered alumina films on NiAl(110).[7,8] In situ infrared reflection absorption spectroscopy (IRAS) is employed in combination with molecular beam methods, which allow us to acquire spectra over a broad range of well-defined conditions.[11] Previously, these systems have been characterized in detail with respect to their electronic and geometric structure and their adsorption properties (see refs 9 and 10 and references therein). In addition, the kinetics and mechanism of several model reactions have been investigated.[11-14]

In this work we address two questions: (i) the type and the fraction of particle facets on both types of systems (model thin films vs supported polycrystalline oxides) responsible for CO absorption and (ii) the nature and the proportion of defect sites on faces of polycrystalline samples prepared utilizing different precursors as compared to thin films.

On the basis of these results the role of the different supports with respect to the reactivity toward methanol will be investigated.[25]

2. Experimental Section

MgO-supported palladium catalysts (2.5, 5, and 10 wt %) were prepared by impregnation of $Mg(OH)_2$ either with solutions of palladium chloride or with solutions of $[Pd(NH_3)_4](NO_3)_2$ (5% Pd by weight) and then dried at 403 K overnight and the first ones calcined in air at 773 K for 4 h.

Al_2O_3-supported palladium catalysts (2.5 wt %) were prepared by impregnation of $\gamma-Al_2O_3$ with solutions of palladium chloride and then dried at 403 K overnight.

Then all the samples were transferred to IR quartz cell, where they were treated at 623 K and finally reduced at different temperatures ranging up to 723 and 773 K.

The $Pd/Al_2O_3(\gamma)$, Pd/MgO(Cl) and $Pd/MgO(NO_3)$ outgassed samples were then dosed with CO ($p = 40$ Torr) and the FTIR spectra were recorded at 300 K in situ at 2 cm^{-1} resolution, using a Bruker IFS 28 spectrometer, equipped with a cryogenic MCT detector. The pressure was then gradually reduced in steps from 40 to 10^{-4} Torr. After each step the FTIR spectrum of adsorbed CO species was obtained. The final spectrum corresponds to CO species irreversibly adsorbed at 300 K. Inspection of literature data suggests that the coverage of irreversible species on (100) and (111) facets is around 0.5.[2,3] On this basis the sequence of spectra obtained in the 40 to 10^{-4} Torr interval corresponds to coverages in the 0.5-1 interval. The procedure described above does not allow us to obtain the spectra of adsorbed CO in the 0-0.5 interval. This must be kept in mind when comparison with the spectra of CO on single crystals and on model systems (vide infra) is made.

The morphological characterization has been carried out by transmission electron microscopy (TEM; JEOL JEM 200 EX and Philips CM 200 FEG operated at 200 kV) and atomic force microscopy AFM (Park Scientific Auto Probe LS, equipped with an high aspect ratio silicon conical tip and operating in contact and noncontact mode).

IRAS experiments on the single-crystal based model catalyst have been performed in a combined molecular beam/IRAS apparatus.[26] The molecular beam system combines several independent beam sources, angular-resolved and -integrated gas-phase detection and in-situ time-resolved IRAS. The spectra in Figure 8a,e, have been recorded in a second UHV system, which was designed for IRAS, XPS (X-ray photoelectron spectroscopy) and STM (scanning tunneling microscopy) measurements.

The alumina film was prepared by sputtering and annealing of a NiAl(110) single crystal, followed by an oxidation and annealing procedure.[7,8,27] Cleanliness and quality of the oxide film was checked via LEED (low energy electron diffraction) and AES (Auger electron spectroscopy). Before the experiment, the Pd (>99.9%) was deposited under UHV conditions using a commercial evaporator (Focus, EFM 3). Details concerning the preparation conditions are given elsewhere.[28]

Via choosing the appropriate preparation parameters, the structure, size, and density of the Pd aggregates can be controlled (see ref 9 and references therein).

Here, we choose two principal sets of preparation conditions: (a) The first type of Pd model surfaces (in the following denotes as type I Pd particles) is prepared by depositing Pd at a sample temperature of 300 K. (b) As a second type of Pd particles, we investigate aggregates, which were formed by Pd deposition at a sample temperature of 100 K.

Except for samples prepared at 90 K (Figure 8a,e), the Pd particles were stabilized by oxygen and CO exposure after preparation, as discussed previously.[29,30] The IR spectra were acquired using a vacuum FT-IR spectrometer (Bruker) at a spectral resolution of 2 cm^{-1}. The IR spectra taken during CO oxidation (Figure 8c,d,g,h) were recorded at an effective pressure of 10^{-6} mbar in a CO−oxygen mixture (prepared by overlapping molecular beams of CO and oxygen at the sample position) at

Surface Reactivity of Pd Nanoparticles

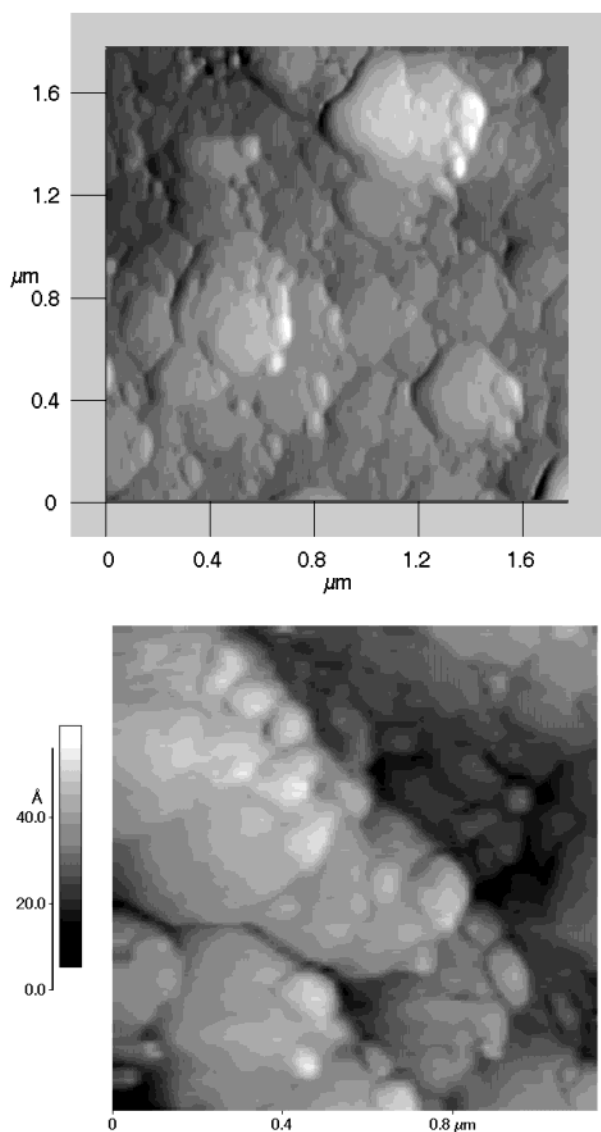*J. Phys. Chem. B, Vol. 108, No. 11, 2004* **3605**

Figure 1. NC-AFM images of Pd particles aggregates (60−90 nm in size) on polycrystalline MgO surfaces (Pd 10 wt %).

different fractions of CO (x_{CO}) in the total beam flux impinging on the sample (see, e.g., refs 28 and 31). In all other experiments, CO was applied by means of a gas doser, effusive beam source of supersonic beam source.

3. Results and Discussion

3.1. Morphological Characterization. *3.1.1 Polycrystalline MgO Supported Pd Crystallites.* From NC-AFM (non contact atomic force microscopy) images a top view of Pd/MgO(Cl) samples (10 wt %) is given. It is found that most Pd particle aggregates are grown on polycrystalline MgO surfaces and they are 60−90 nm in size (Figure 1). From these preliminary AFM results it can be noticed that a high degree of Pd particles dispersion on MgO terminations is occurring: this means that Pd aggregates are located mainly on defective positions such as edges, steps, and corners.

However, only the presence of agglomerates with their distributions can be evidenced because of low resolution conditions, whereas the shape and structure of single particles can be obtained by electron microscopy (Figure 2).

Figure 2 shows a comparison of Pd/MgO samples obtained from the two different precursors. For Pd/MgO(Cl) (Figure 2a) a mean Pd particle diameter of 15 ± 3.5 nm was determined

(analyzing ∼100 particles). The inset in Figure 2a shows several Pd particles with polygonal outlines and straight edges, suggesting the presence of low-index facets. The majority of particles has contours that can be described in terms of cubooctahedral shapes suggesting a strong contribution of (100) and (111) faces on Pd/MgO(Cl). However, the corners are typically truncated, leading to a somewhat "rounded" appearance at low magnification. Pd particles located at thin edges of the MgO support (such as those in Figure 2a marked by arrows) sometimes allow side-on views and a height/diameter aspect ratio of ∼0.6−0.75 was found, illustrating the 3d nature of the particles.

For Pd/MgO(NO₃) (Figure 2b), the mean Pd particle diameter was about 11 ± 4.5 nm and particularly Pd particles with a diameter below 10 nm showed rather irregular profiles (i.e., neither polygonal nor rounded). Figure 2 also indicates that on Pd/MgO(NO₃) the total Pd loading was higher than on Pd/MgO(Cl), which explains the intensity difference of the IR spectra of the two samples (see below).

The crystallinity of the Pd particles was evident from electron diffraction. The inset in Figure 2b shows a typical ring pattern of randomly oriented metal particles, with similar patterns being observed for both types of catalysts. The "broken-up rings" consist of reflections originating from many Pd particles and indicate Pd {111}, {200}, and {220} interplanar distances, besides reflections from MgO (e.g., at ∼0.24 nm).

Images on Pd/γ-Al₂O₃ (not reported for the sake of brevity) show irregularly shaped Pd particles, with sizes in the 8−15 nm range.

3.1.2. Single-Crystal Based Pd Model Catalysts. On Pd model surfaces prepared by depositing Pd at a sample temperature of 300 K (I Pd particles) large and ordered crystallites are formed (Figure 3a). These nanocrystallites grow in (111) orientation, preferentially exposing (111) facets as well as a very small fraction of (100) facets. Specifically, we choose a nominal Pd coverage, which results in the formation of crystallites containing approximately 3000 Pd atoms (average particle size of approximately 6 nm).

Pd model surfaces prepared by depositing Pd at a sample temperature of 100 K (II Pd particles) are characterized by a higher nucleation density, and consequently, the formation of smaller particles at similar nominal metal coverage (Figure 3b). On these smaller aggregates no indications for the formation of ordered crystal facets could be found and it is assumed that their surface structure is characterized by a high density of defect sites. Specifically, we choose systems with particle sizes between 400 and 900 atoms per aggregate. More details concerning the preparation and structure of the two types of model systems can be found in the literature.[9,28,29,40]

3.2. FTIR Spectra of CO Adsorbed on Pd/γ-Al₂O₃ Systems. FTIR spectra of CO adsorbed at 300 K on Pd/γ-Al₂O₃ systems are shown in Figure 4a,b. Two absorptions centered at $\nu = 2070$ and 1920 cm^{-1} are observed at $\theta = \theta_{max}$, whose intensity changes with the thermal treatment as a consequence of the increase of the dimensions and regularity of the metal particles (images not reported for the sake of brevity). The frequency value of the band at $\nu = 2070$ cm^{-1} is very similar to those found on Pd/MgO(Cl) and Pd/MgO(NO₃) samples, which, as discussed in the following, is ascribed to linearly bonded CO on edges, steps, or terraces of (100) and (111) facelets. As far as the second band at $\nu = 1920$ cm^{-1} is concerned, we observe that it is unusually broad. We consequently associate it with different types of CO species on heterogeneously distributed 3-fold hollow sites due to hollow
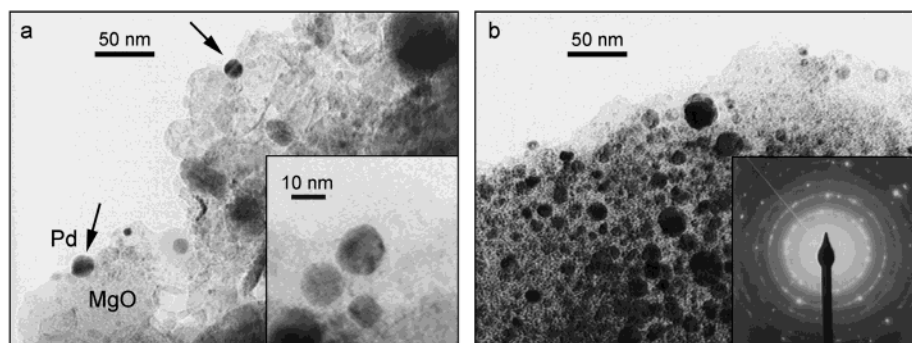
Figure 2. Transmission electron micrographs of Pd particles on polycrystalline MgO surfaces (2.5 wt % Pd): (a) Pd/MgO(Cl) (inset: particles with various shapes in higher magnification); (b) Pd/MgO(NO₃) (inset: typical electron diffraction pattern; see text).
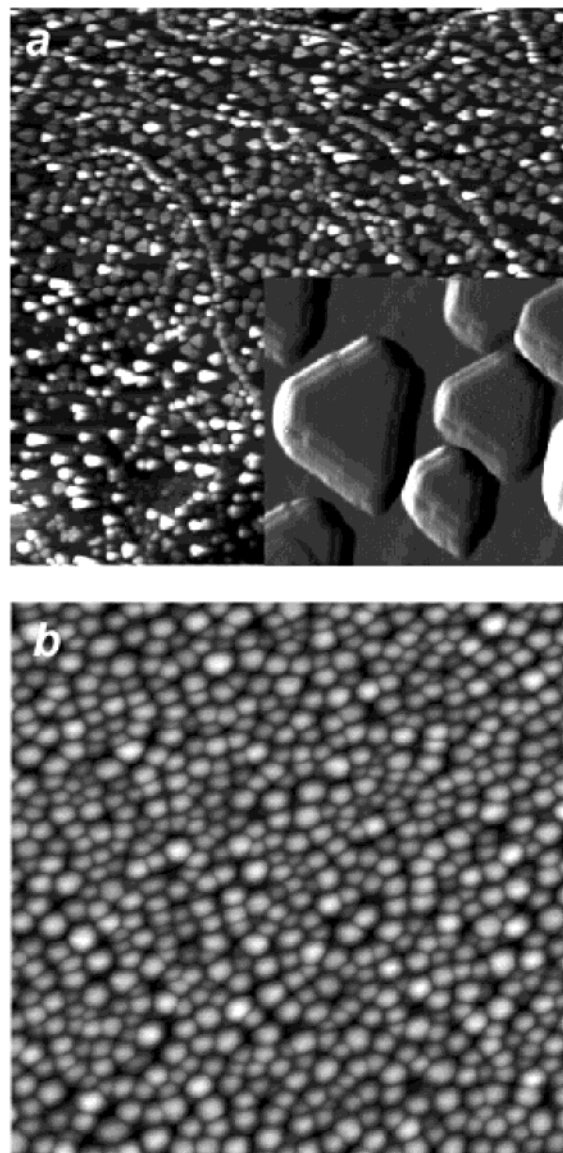

Figure 3. (a) Pd model catalyst of type I: STM image (3000 Å × 3000 Å) of Pd particles (approximately 3000 atoms/particle) grown at 300 K on Al₂O₃/NiAl(110). The inset shows a differentiated close-up STM image of the particles (200 Å × 200 Å).[29] (b) Pd model catalyst of type II: STM image (1000 Å × 1000 Å) of Pd particles (approximately 200 atoms/particle) grown at 90 K on Al₂O₃/NiAl(110) after heating to 500 K.[32]

CO. This attribution is consequently the same and it is in agreement with the high intensity of the 2070 cm^{-1} band (because on poorly defined microcrystals the concentration of
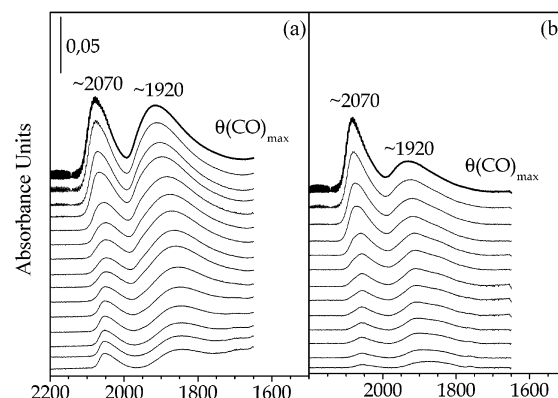

Figure 4. FTIR spectra in the CO stretching region from 2200 to 1500 cm^{-1} of CO adsorbed at 300 K on Pd/γ-Al₂O₃ (2.5 wt %) outgassed and reduced (a) at 623 K and (b) at 773 K (θ_{max}, $p(CO) = 2.66$ kPa; θ_{min}, $p(CO) \rightarrow 0$).

edges and steps is highest). The attribution of the 2070 cm^{-1} is also in agreement with the observed remarkably large half-width, which is indicative of high heterogeneity. We anticipate that the spectra illustrated in Figure 4 are remarkably different from those of CO adsorbed on Pd/MgO systems and Pd/film (vide infra).

This is due to the fact that Pd particles supported on the disordered γ-Al₂O₃ substrate (a solid with defective spinel structure) are characterized by ill-defined morphology and expose facets of low dimension with high concentrations of defects. For these reasons, results on Pd/MgO systems will be discussed preferentially and compared with those obtained on thin films.

3.3. FTIR Spectra in the Carbonyl Region of CO Adsorbed on Pd/MgO(Cl) and Pd/MgO(NO₃) Systems. FTIR spectra of CO adsorbed at 300 K on PdMgO(Cl) and Pd/MgO(NO₃) systems are shown in Figure 5. On this figure two spectral sequences are simultaneously reported: the CO stretching regions from 2200 to 1500 cm^{-1} for the Pd/MgO(Cl) system (top) and the same region for the Pd/MgO(NO₃) (bottom).

On both Pd/MgO systems a remarkable decrease of the intensity of the bands is occurring in the 2200–1500 cm^{-1} region, as a consequence of the progressive sintering procedure.

This is due to the progressive increment of the particle dimension and to the associated more well-defined particle shape (because the thermal treatments at increasing temperature favor the formation of Pd microcrystals exposing the most stable low index (100) and (111) faces. The simultaneous increment upon sintering of crystallite dimension and regularity is explaining the progressive decrease of the intensity of the bands of adsorbed CO and the gradual simplification of the spectra illustrated in Figure 5a–d and Figure 5e–h.
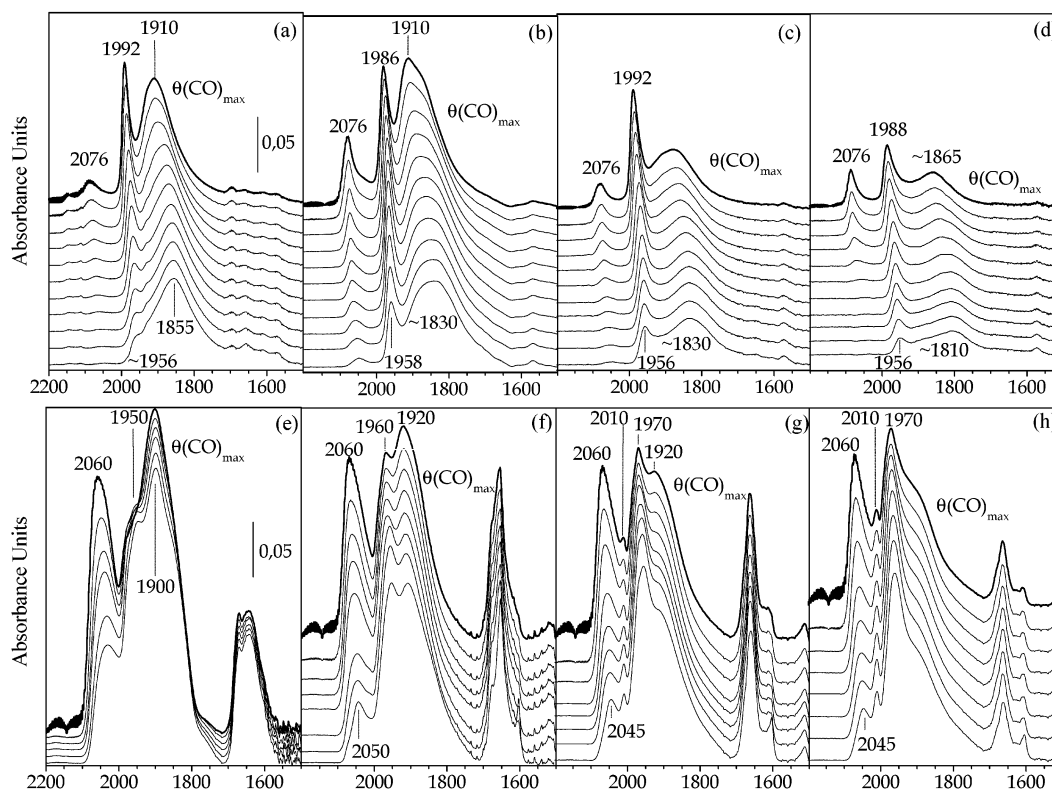
Surface Reactivity of Pd Nanoparticles

J. Phys. Chem. B, Vol. 108, No. 11, 2004 **3607**

Figure 5. (a)−(d) FTIR spectra in the CO stretching region from 2200 to 1500 cm^{-1} of CO adsorbed at 300 K on Pd/MgO(Cl) (2.5 wt %) outgassed at 623 K and reduced at progressively higher temperature: (a) at 373 K; (b) at 523 K; (c) at 623 K; (d) at 773 K (on the top). (e)−(h) FTIR spectra of CO adsorbed at 300 K on Pd/MgO(NO$_3$) outgassed at 623 K and reduced (e) at 523 K and (f) at 623 K and outgassed and reduced (g) at 673 K and (h) at 723 K (θ_{max}, p(CO) = 2.66 kPa; θ_{min}, p(CO) → 0).

3.3.1. CO Adsorption on Pd/MgO(Cl) System. By considering, in greater detail, the sequences reported in Figure 5a−d, corresponding to FTIR spectra of decreasing doses of CO adsorbed on Pd/MgO(Cl) systems, we notice two distinct narrow bands (at $\nu \cong$ 2076−2050 and 1992−1956 cm^{-1}), the last one with full width at half-maximum ($\cong$50 cm^{-1}) comparable to the figures usually obtained for CO adsorbed on Pd particles supported on (100) MgO single crystals,[4−5] on metal particles supported on films obtained in RAIRS experiments[6] and on (100) and (111) faces of single crystals.[2,3] These two absorptions are assigned to linearly bonded (band at $\nu \cong$ 2076−2050 cm^{-1}) and bridge-bonded (band at $\nu \cong$ 1992−1956 cm^{-1}) CO species, adsorbed on Pd (100) and (111) facets, in agreement with the results obtained on model catalysts.[1−6] These bands shift to lower frequencies (2076 → 2050, $\Delta\nu \cong$ 26 cm^{-1}, and 1992 → 1956, $\Delta\nu \cong$ 36 cm^{-1}) by decreasing the CO coverage. This shift is due to changes of lateral interactions, as the layer becomes less and less dense. The shifts are smaller than those found on single-crystal faces.[3] This is due to (i) the reduced extension of the (100) and (111) facets, which explains the observed reduction in the magnitude of the lateral interactions within the adlayer and (ii) to the smaller coverage-dependent changes observed in the adopted experimental procedure (0.5 $\leq \theta \leq$ 1). In respect to this, we notice that our spectra are very similar to those obtained at the highest coverages on Pd/films and single crystals.

The higher values of the ν(CO) of species adsorbed on Pd/MgO(Cl) are consistent with either a higher dipole−dipole interaction associated with the large extension of the facets, either a lower back-donation of metal electrons into the antibonding CO 2π^* orbital, a fact that also justifies the more pronounced reversibility upon reducing the CO pressure at 300 K. We think that both effects are contributing. A plausible

explanation of the lower back-donation could be that Cl atoms adsorbed on the matrix/Pd interfaces subtract electron density from the Pd particles and hence decrease their ability to back-donate electron density to adsorbed CO. We have a clear demonstration of the role of the support in affecting the adsorption properties of Pd particles.

The 2076 cm^{-1} band, assigned to weakly bonded linear species, is observed at high CO coverage, when the molecules are forced in the top position, due to "compression" effects. The broad character of this feature (when compared to single crystals) indicates that CO species on both (100) and (111) faces are contributing. A contribution of linear species adsorbed on edges and terraces is not excluded.

The high intensity and the small fwhm of the band at 1992−1956 cm^{-1}, assigned to bridge-bonded CO species suggests that the metal particles on these polycrystalline systems expose faces with a high level of regularity, as supported from the analyses of TEM images.

Another broad and complex band is present in the $\nu \cong$ 1920−1800 cm^{-1} range. This band is readily ascribed to CO adsorbed on different types of 3-fold hollow sites. This absorption is plausibly complex and it is constituted by two components, which are affected by thermal treatments in a different way. On samples treated at 773 K only one of the components is observable ($\nu \cong$ 1865 cm^{-1} at θ_{max}). A remarkable feature, well evident in Figure 5b,c, is that, on evacuation, the bands shift to lower frequency, without loss of intensity. This means that (i) the concentration of the species is not substantially decreasing upon reducing the CO pressure at 300 K, because they are more strongly adsorbed than the linear and the bridge ones and (ii) the shift is plausibly caused by the gradual modification of the surroundings of the 3-hollow sites (for instance because the
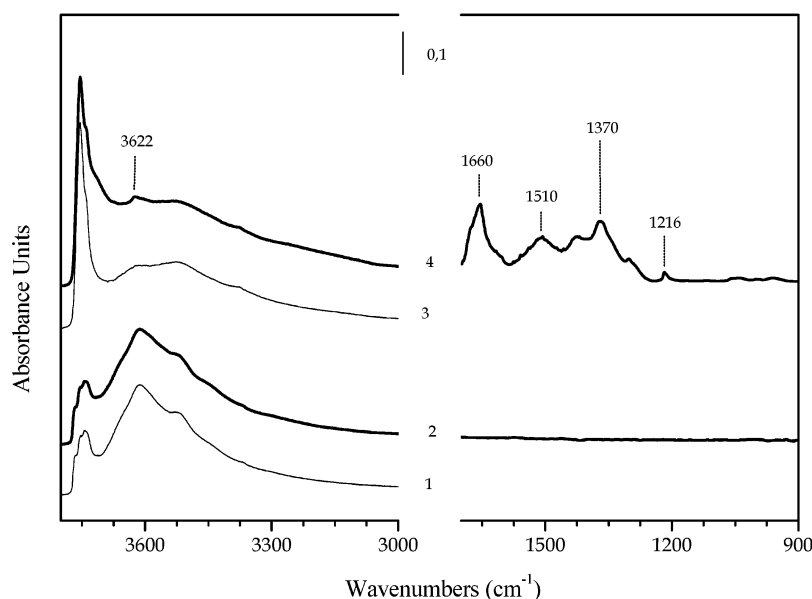
Figure 6. FTIR spectra in the 3800−3000 and 1700−900 cm^{-1} ranges. Curves 1 and 3 show the spectra before CO adsorption on Pd/MgO(Cl) and Pd/MgO(NO$_3$), respectively; curves 2 and 4 show the spectra at θ(CO)$_{max}$ ($p = 2.66$ kPa) on Pd/MgO(Cl) and Pd/MgO(NO$_3$), respectively.

concentration of linear and bridge species in adjacent positions is gradually changing).

3.3.2. CO Adsorption on Pd/MgO(NO$_3$) System. Coming now to the FTIR spectra of CO adsorbed on Pd/MgO(NO$_3$) systems (bottom of Figure 5) very intense bands in the 2200−1500 cm^{-1} region are observed, which look very similar to those found on the Pd/MgO(Cl) systems. By analogy with Pd/MgO(Cl) the two groups of bands at $\nu \cong$ 2060−2025, 1970−1950, and 1920 cm^{-1} are assigned to linear, bridge-bonded species, and 3-fold hollow sites.

A detailed analysis of the spectra allows us to conclude (i) all the observed bands are more intense, less reversible, and shifted to lower frequency, as discussed before; (ii) most of the components are broader, with distinctly higher half-widths; and (iii) a new component not present on the Pd/MgO(Cl) system is observed at 2010 cm^{-1}, which we anticipate to be associated with CO species adsorbed on carbided areas of the Pd surfaces, i.e., the areas involved in the CO disproportion.

All these facts confirm that the Pd dispersion on Pd/MgO(NO$_3$) is higher than on Pd/MgO(Cl), the Pd particles are smaller and their shape less defined, with a relevant concentration of edges, steps, and corner sites, in agreement with the results obtained from TEM analysis.

With the dimensions of the flat terraces being smaller on the Pd/MgO(NO$_3$) system, the dipole−dipole coupling (responsible for the shift to higher ν) is also partially suppressed, as testified by the smaller shift of the CO frequencies induced by the change of CO coverage.

Another aspect deserving a specific remark is related to the absence of the spectral features in the 1900−1800 cm^{-1} range, typical of different types of 3-fold hollow sites, already observed on Pd/MgO(Cl) samples.

Besides the experiments described in Figure 5, obtained by initial saturation of the Pd surface with CO and successive outgassing at 300 K, other spectral sequences have been obtained by following the reverse procedure (the spectral features correspond to sequential doses of CO). Unfortunately, the sequence of spectra obtained in this way are affected by diffusion problems, which prevent a uniform distribution of CO. For this reason these data are not discussed in detail.

3.3.3. FTIR Spectra in the Hydroxyl and Carbonate Species Region. The most remarkable differences between the Pd/MgO(NO$_3$) and Pd/MgO(Cl) samples are observed in the 3800−3200 and 1770−900 cm^{-1} ranges (Figure 6), where surface carbonate and bicarbonates are absorbing.

Two of these differences, in particular, are mentioned: (i) On Pd/MgO(NO$_3$) a clear band at 3752 cm^{-1} is observable, which is by far less intense on Pd/MgO(Cl). This band is assigned to surface hydroxyl species of the MgO support. The lower intensity on Pd/MgO(Cl) is likely associated with the presence of Cl$^-$ ions on the surfaces, which substitute the OH$^-$ groups and lead to OHs modified by hydrogen bonding; the presence of residual Cl$^-$, hypothesized before on the basis of the spectra of CO on Pd particles, is confirmed in this manner. (ii) On Pd/MgO(NO$_3$) two pairs of bands in the 1660−1300 cm^{-1} range ascribed to surface carbonate and bicarbonate species are observed upon CO dosage. These species were not found on Pd/MgO(Cl). The small peaks at 3622 and 1216 cm^{-1} are the ν(OH) and δ(OH) modes of surface bicarbonates. All these species are likely adsorbed on the MgO matrix.[33]

The presence of carbonate and bicarbonate groups indicates that on Pd particles disproportionation of CO is occurring (2CO → CO$_2$ + C). The carbon remains on Pd particles as a carbide, whereas CO$_2$ reacts with basic O^{2-} and OH$^-$ ions of the MgO surface to give CO$_3{}^{2-}$ and HCO$_3{}^-$. In favor of this hypothesis, let us mention that temperature programmed desorption (TPD) experiments, used to monitor the CO adsorption capacity during cycles of CO adsorption/desorption over small palladium particles deposited on MgO substrates,[34] have demonstrated that CO desorption is accompanied by CO$_2$ production, resulting from CO disproportion on the Pd surface. Carbon is stabilized on the metal particles. Indirect evidence of the presence of C have been obtained by the vibrational spectra of adsorbed CO. As a matter of fact, on Pd/MgO(NO$_3$) the narrow band at 2010 cm^{-1}, being absent on Pd/MgO(Cl), can be readily assigned to CO adsorbed on carbided areas of the Pd surfaces.

Carbonate and bicarbonate species are not observed on Pd/MgO(Cl). This is certainly associated with the less basic character of the MgO doped with Cl, which can inhibit the adsorption of CO$_2$ formed by disproportion of CO on Pd
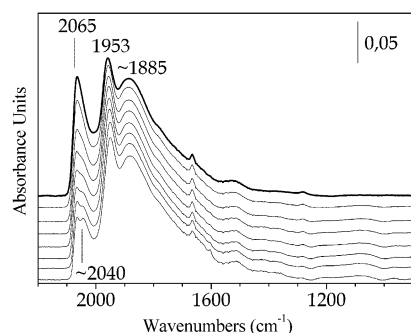
Surface Reactivity of Pd Nanoparticles

J. Phys. Chem. B, Vol. 108, No. 11, 2004 **3609**

Figure 7. FTIR spectra in the CO stretching region from 2200 to 900 cm^{-1} of CO adsorbed at 300 K on precovered hydrogen Pd/MgO(NO$_3$) outgassed and reduced at 673 K (θ_{max}, p(CO) = 2.66 kPa; θ_{min}, p(CO) → 0).

particles. However, the absence of any evidence of C on Pd/MgO(Cl) suggests that on the chlorine doped system the disproportion of CO is strongly suppressed. We can only speculate about the reasons of this suppression. Two hypotheses can be advanced: (i) the disproportion of CO needs metal/support cooperation, the surface basicity of MgO behaving actively in stabilizing one of the products (CO$_2$) of the reaction, and (ii) the CO disproportion occurs only on very small Pd particles (more favored on Pd/MgO(NO$_3$)).

For the time being, no definitive conclusions can be drawn on the origin of this effect.

3.3.4. Effect of H$_2$ Preadsorption on CO/PdMgO(NO$_3$) Systems. Figure 7 shows the FTIR spectra in the 2200−900 cm^{-1} region of CO adsorbed on hydrogen precovered samples. The hydrogen adsorption was obtained by dosing H$_2$ at 623 K, then by cooling at 300 K in H$_2$ atmosphere, and by successive outgassing at RT.

By comparing these results with those obtained on hydrogen-free samples (Figures 5g and 6, curve 4), one can see many changes. As a matter of fact, the complex band in the 1660−1300 cm^{-1} range, which has been ascribed to the presence of carbonate and bicarbonate ions adsorbed at the surface of MgO, is negligible after hydrogen preadsorption. Furthermore, the band attributed to CO adsorbed on carbided surfaces at 2010 cm^{-1} is absent. This means that in the presence of preadsorbed hydrogen the disproportionation reaction is largely inhibited. The presence of hydrogen species on the Pd/MgO(NO$_3$) surface is affecting also the spectrum of carbonylic species. In particular, the band at 1920 cm^{-1} due to CO species adsorbed on 3-fold hollow sites is apparently absent.

3.4. IRAS Spectra of CO Adsorbed on Pd Model Systems. *3.4.1 IR Spectra of Adsorbed CO: Structure and Temperature Dependence.* An overview over the IR reflection absorption spectra of the CO stretching frequency region is given in Figure 8. The spectra were recorded as a function of CO coverage at sample temperatures between 90 and 465 K for both types of model systems. The spectra at 90 and 300 K were acquired after successively dosing CO at the respective temperature.

Only the spectra taken at 300 K can be usefully compared with those obtained on polycrystalline Pd/MgO and Pd/Al$_2$O$_3$ samples. Notice that the maximum equilibrium pressure reached on dispersed samples is much higher. This means that the spectra of Figure 8b (300 K) must be compared with the less intense spectra of Figure 5 (because the equilibrium pressures of CO are comparable).

The spectra at 415 and 465 K were measured during CO oxidation in a CO−oxygen mixture at different fractions of CO (x_{CO}: fraction of CO in the total gas flux). Details concerning the experimental procedure can be found elsewhere.[28]

For the type I particles (large ordered crystallites prepared at 300 K) at temperatures of 415 K (Figure 8c,g) and 465 K (Figure 8d,h), two absorption features at 1820 and 1895 cm^{-1} are observed, which shift to approximately 1850 and 1925 cm^{-1} with increasing CO coverage. The intensity ratio of both peaks depends on the CO coverage with the high-frequency feature dominating at high coverage. At 300 K and below (Figure 8a,b) additional CO can be adsorbed under UHV conditions, giving rise to adsorption bands in the range between 2000 and 1950 cm^{-1} as well as at 2070 and 2108−2087 cm^{-1}.

If we compare the CO spectra for the smaller particles of type II (Figure 8e−h) to those of type I (Figure 8a−d), only minor differences are observed at high sample temperature (415−465 K). One dissimilarity is the weaker change in relative intensity for the two features around 1820 and 1920 cm^{-1} as a function of coverage, which has been discussed previously.[28] Similar to the case for the type I particles, additional absorption bands appear for adsorption at 300 K and below in the regions around 2000−1970 and 2120−2070 cm^{-1}. In the latter spectral region, however, a strongly enhanced absorption for the type II particles indicates a pronounced particle structure dependence.

To some extent, the spectra can be interpreted on the basis of Pd (111) single-crystal data, where a large number of adsorbate structures are formed as a function of the coverage. In particular, various ordered structures are observed in the 1920 and 1800 cm^{-1} region, corresponding with CO occupying a mixture of fcc and hcp hollow sites.[35−41]

As far the 2000−1950 and 2120−2070 cm^{-1} spectral regions are concerned, major differences are observed as compared with the CO/Pd(111) reference. In the following, we will consider these regions in detail.

The bands in the region between 2000 and 1950 cm^{-1} can be attributed to bridge-bonded CO, which, in contrast to CO/Pd(111), are observed over the full temperature range from 100 K up to temperatures exceeding 300 K. Previously, we have discussed two possible assignments of these CO bands: (a) bridge-bonded CO adsorbed on Pd(100) microfacets and (b) bridge-bonded CO adsorbed at defect sites, such as particle edges or steps on the particle facets.[42,43] It was argued that due to the small fraction of the (100) facets and their tilted geometry, however, the contribution of CO on (100) facets can be expected to be minor (note that the metal surface selection rule, which suppresses excitation of dipoles oriented parallel to the surface, is also valid for sufficiently thin metal−supported oxide films[44]). The resulting assignment to mainly particle edge, steps, or other defect sites was recently corroborated by theoretical investigations.[10]

A closer inspection of the bridge-bonded CO region as a function of CO coverage and particle structure (Figure 8a,b,e,f) reveals strong coverage dependent effects. On the other hand, the dependence on the particle structure (type I versus type II) is only moderate.

As a function of the CO density, strong frequency shifts as well as multiple absorption features appear in this region. In more detail, this is shown in the spectra in Figure 9a, which have been acquired after CO saturation at slightly different sample temperatures. The exact origin of the different features is unclear yet. Possible explanations include, e.g., contributions from (100) facets, energetically different adsorption sites at particle defects (e.g., steps, interface sites and edges) and transformations between adsorbate structures of different densities at particle edges or defects.

The differences observed for the two types of particles include moderate changes in the relative intensity in the region of bridge-
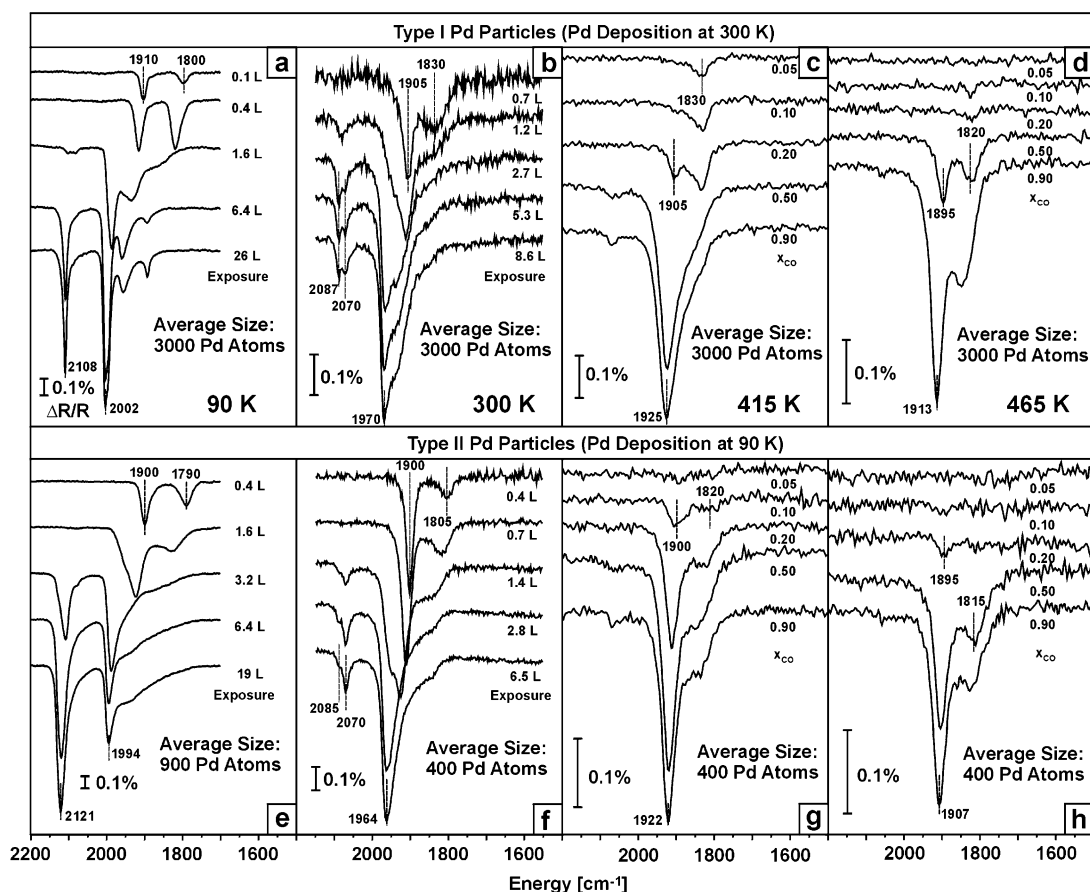
Figure 8. IR reflection absorption spectra for CO adsorbed on different Pd model catalysts: comparison of type I and type II particles and influence of the sample temperature and the CO coverage (see text for details).
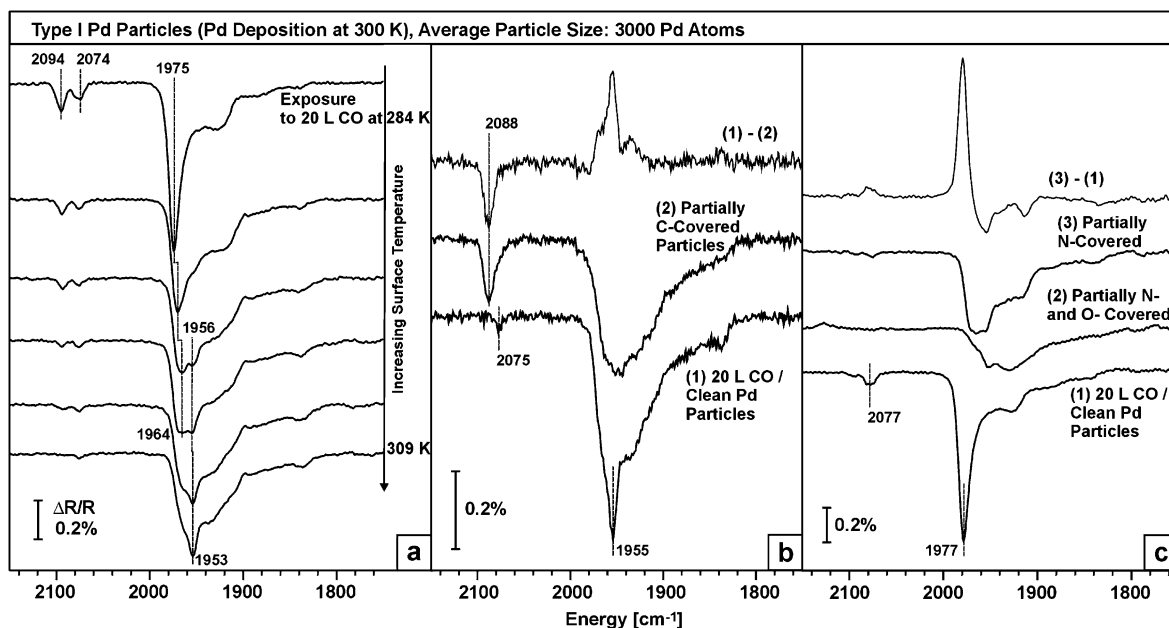

Figure 9. Influence of coadsorbates on the IR reflection absorption spectra for CO adsorbed on a Pd model catalysts of type I (the spectra were recorded at a sample temperature of 100 K after exposure to CO at temperatures around 300 K): (a) clean Pd model catalyst; (b) partially carbon covered catalyst (prepared be methanol decomposition; see text for details); (c) partially oxygen/nitrogen and partially nitrogen covered catalyst (prepared by NO decomposition and CO titration; see text for details).

bonded CO and in the (111) facet region (<1920 cm^{-1}) as well as a slight general blue shift for the smaller particles. The latter effect can be easily explained by taking into account the higher density of bridge-bonded CO at defect sites leading to enhanced dipole coupling effects. In addition, chemically induced shifts are expected due to the known particle size dependence of the Pd—CO bonding strength (see, e.g., refs 9 and 45).

More surprising is the relative intensity behavior in the bridging CO and Pd(111)-facet region, which does not reflect the strongly enhanced edge and defect density for the smaller

Surface Reactivity of Pd Nanoparticles

J. Phys. Chem. B, Vol. 108, No. 11, 2004 **3611**

and less ordered particles of type II. In fact, the bridging CO region strongly dominates over the lower frequency bands at adsorption temperatures of 300 K and below in a similar way for all particles sizes. This behavior is mainly attributed to dipole coupling effects between neighboring oscillators, which depend on the distribution and frequency of the oscillators, but in all cases leads to a pronounced intensity transfer to the high frequency band, i.e., the bridge-bonded CO.[44,46] In addition, a contribution due to variations of the dynamic dipole moment for different absorption sites cannot be excluded.

On the basis of these observation it follows that the frequency region between 2000 and 1950 cm^{-1} is not only indicative of certain Pd crystal planes such as (100) facets but is in a very prominent way also characteristic of specific sites on the Pd particles such as edges, steps-like sites or other types of defects. The complex coverage dependent behavior, however, does not permit an unambiguous assignment to such sites without additional structural information on the particle morphology. In addition, a quantification of the relative densities of the corresponding adsorption sites is precluded by strong coupling effects.

Next, we consider the bands in the region between 2120 and 2070 cm^{-1}, which can be attributed to CO adsorbed in an on-top geometry. Here, we observe two separate bands: a weak feature around 2070 cm^{-1}, which saturates around 300 K, and a second feature between 2120 and 2085 cm^{-1}, which starts being populated at temperatures around 300 K and strongly dominates at lower temperatures (see Figures 8a,b,e,f and 9a).

Taking into account the differences in comparison with CO/Pd(111), we tentatively assign the band at 2070 cm^{-1} to on-top CO bonded to specific rare defect sites such as, e.g., particle corners, whereas the high-frequency band between 2085 and 2120 cm^{-1} has to be attributed to an on-top CO species with high abundance and enhanced binding energy. On the basis of the morphology of the particles and the size and structure dependence, we assign this feature to on-top CO at particle edge sites, steps, and other defects providing similar local adsorption geometry.

This assignment is consistent with the spectra obtained on Pd/Al$_2$O$_3$(γ) (Figure 4) and Pd/MgO (Figure 5), where this absorption is dominant, because the number of defect sites is very high.

In contrast to the bridge-bonded CO region, the on-top CO shows a rather simple behavior as a function of CO coverage and particle structure. A single peak is found in the high frequency region showing a blue shift of approximately 30 cm^{-1} with increasing coverage (due to dipole and chemical coupling effects as well as differences between the local adsorption sites). The absence of multiple features indicates more well-defined local adsorption sites and less structural flexibility in the adsorbate layer.

What appears most surprising, however, is that upon saturation at 100 K the relative intensity of the high-frequency on-top band qualitatively reflects the defect density of the particles: as a matter of fact, the feature is most intense for small and/or defect rich particles (such as type II) and decreases with the increasing size of well-ordered crystal facets (i.e., for large particles of type I) (for comparison see also refs 9 and 43). With respect to the use of CO as a structural probe we may conclude at this point that a close inspection of the on-top absorption bands, and their temperature and coverage dependent intensity behavior, may indeed provide qualitative information in the size and the morphology of supported Pd particles.

3.4.2. IR Spectra of Adsorbed CO: Influence of Coadsorbed Atomic Carbon. The CO spectra obtained on the pristine Pd
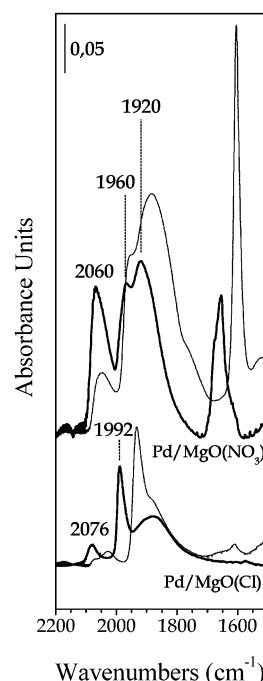
Figure 10. FTIR spectra in the CO stretching region from 2200 to 1500 cm^{-1} of CO adsorbed at 300 K on Pd/MgO(Cl) (2.5 wt %) and Pd/MgO(NO$_3$) samples outgassed and reduced at 623 K. Continuous curves refer to CO adsorbed on bare samples. Dotted curves refer to CO adsorbed on partially carbon covered samples (prepared by methanol decomposition; see text for details).

particles and after partial contamination by atomic carbon are displayed in Figure 9a,b. The carbon deposits are formed by C−O bond scission during methanol decomposition, as described in a previous contribution.[12]

To enhance the spectral resolution (see also refs 12 and 47), an experimental procedure, which involves CO saturation at a well-defined sample temperature typically around 300 K, was applied and subsequent acquisition of the IR spectrum at 100 K was carried out.

On the partially carbon covered sample (Figure 9b), only weak changes occur in the spectral region (2) corresponding to CO adsorption at hollow sites on the particle facets. The most apparent change is the strong loss of bridge-bonded CO (2) attributed to adsorption at particle edges, steps, or defects. This behavior indicates that the adsorption at the particle edge and defects sites is preferentially modified by the presence of the atomic coadsorbates, suggesting that the carbon atoms are preferentially located in the vicinity of these defects rather than on the ordered facets of the particles. This observation is consistent with a recent STM study of oxygen adsorption on the same Pd model catalyst, showing preferential adsorption at particle edges.[48]

In addition to the effects in the bridge-bonded region, a surprising effect is observed in the spectral region of on-top CO for carbon precovered as compared to nitrogen/oxygen precovered Pd particles (Figure 9c): whereas nitrogen and/or oxygen precoverage leads to a simple loss of the bridging CO only, carbon contamination additionally results in a strong increase in bands corresponding to CO adsorbed in on-top geometry (2088 cm^{-1}). Note that this effect is not due to the slightly different adsorption temperatures but can be observed over a broader temperature and coverage range (see, e.g., ref 10). It is concluded that the carbon coadsorbate leads not only to poisoning and depopulation of bridge sites at particle defects but also to a population of on-top sites in the vicinity of defects

(possibly due to a reduced intermolecular repulsion at the CO depleted edges). Possible explanations for the dissimilarities between the influence of carbon and nitrogen/oxygen co-adsorbates may be related to differences in electronegativity of the atomic adsorbates or to different affinities to form subsurface species on Pd.[49,50]

The results do not coincide completely with those shown in Figure 10 for Pd/MgO systems, where spectra of CO on pure (continue lines) and partially carbon covered (dotted lines) samples are compared.

All the same, it should be noted that on partially carbon covered samples the signal associated with the bridge-bonded species seems to be depleted, as a consequence of carbon contamination and in the sense discussed before. In addition, further contributions might be due to the simultaneous presence of (100) facets, having a plausible different behavior under carbon influence. Thus, we conclude that the observed differences could be understood in terms of the particle morphology and of the different experimental conditions as well.

Furthermore, it can be noticed that in the Pd/MgO(NO$_3$) case, the spectroscopic effect of previous methanol decomposition is more consistent. The explanation of this fact is troublesome. We stress that, in addition to the morphology and the different experimental conditions, even the matrix seems to play a role in determining the structure of carbonaceous entities present on Pd particles.

4. Conclusions

A detailed comparison of the IR spectra of CO adsorbed on (1) Pd/Al$_2$O$_3$, Pd/MgO(Cl), and Pd/MgO(NO$_3$) (polycrystalline) supported catalysts on one hand and (2) single-crystal based Pd/Al$_2$O$_3$ model systems on the other reveals a complex behavior. In general, the spectra imply the simultaneous presence of different species of linear, 2-fold and 3-fold bridges sites. Their relative population depends sensitively on adsorbate coverage, particle structure, and surface contaminations.

In the case of the polycrystalline and powder-based catalysts, sintering at progressively higher temperature leads to a simplification of CO species. On sintered samples, it was found that 2-fold bridge sites on (100) and (111) facets (bands in the 2000–1920 cm^{-1} region) and 3-fold hollow sites on (111) facets (1920–1800 cm^{-1}) are predominant, whereas a small proportion of linear species are observed at high coverage on both (100) and (111) surfaces (2100–2000 cm^{-1}). On samples sintered at the lowest temperatures, linear and bridged species adsorbed on defect sites are also predominant.

The IR bands of CO on Pd/MgO(Cl) and Pd/MgO(NO$_3$) are narrower than those observed on Pd/γ-Al$_2$O$_3$. This is due to the more defined crystalline morphology of the MgO particle, which has an influence on the morphology of Pd crystallites. The Pd/Al$_2$O$_3$, Pd/MgO(Cl), and Pd/MgO(NO$_3$) systems are characterized by supports whose basic character varies in the order Al$_2$O$_3$ < MgO(Cl) < MgO. The basic MgO matrix strongly stabilizes CO$_2$ formed by CO disproportionation on Pd^0. The CO$_2$ reacts with basic O^{2-} ions of the MgO surface to give CO$_3^{2-}$ and with the hydroxyl groups of the MgO surface to give HCO$_3^-$.

On well-defined Pd model catalysts prepared in UHV a strong contribution from bridge-bonded CO in the frequency region between 2000 and 1950 cm^{-1} is observed, which shows a complex coverage dependent behavior. Depending on the morphology of the Pd particles, absorption in this region can be assigned either to minority single-crystal facets such as (100) or to defect sites, e.g., particle edges or steps. For the model

catalysts studied, the latter contribution dominates. However, upon variation of the particle structure, we observe no simple relationship between the intensity of the bridge-bonded CO species and the defect density of the Pd aggregates.

On the Pd model catalyst, different on-top CO signals are observed, with a temperature dependence differing from the single crystal behavior. In contrast to the bridge-bonded CO species, the relative intensity of the on-top CO band at saturation qualitatively reflects the defect density of the particles.

No bands ascribed to species anchored to the Al$_2$O$_3$ support are observable. This result greatly differentiate the model system from the dispersed system, where different terminations with highly heterogeneous sites are present.

Concerning the influence of preadsorbed carbon atoms, it has been observed that the most apparent change is the strong loss of bridge-bonded CO attributed to adsorption at particle edges, steps, or defects. This behavior, observed even on polycrystalline system, indicates that the carbon atoms are preferentially located in the vicinity of these defects rather than on the ordered facets of the particles.

Comparing with different coadsorbates such as atomic carbon, nitrogen, and oxygen on the Pd model catalysts, element-specific differences are identified: whereas oxygen and nitrogen result in pure blocking of bridge sites, the presence of carbon gives rise to an additional occupation of on-top sites. Therefore, the spectral changes not only are indicative of the location of the contamination on the particle but also in some cases may even allow a differentiation between chemical species. However, it remains difficult to distinguish between morphological and chemical influences and supplementary information on the surface structure is indispensable in most cases.

In conclusion, from the comparison of polycrystalline with thin films data, the following main points can be evidenced:

(i) On both systems, apart from the type of matrix, signals in the same spectral ranges denote the presence of the same species adsorbed on a majority of (111) facets and a minority of (100) facets, although a major complexity on polycrystalline systems can be observed due to a different proportion in the particle terminations.

(ii) On both systems, contaminants (e.g., carbon atoms) are preferentially located in the vicinity of edges, steps, or defects rather than on the ordered facets of the particles;

(iii) Carbonate and bicarbonate species are observed on polycrystalline Pd/MgO(NO$_3$), the surface basicity of MgO behaving actively in stabilizing one of the products (CO$_2$) of the disproportion of CO. This reaction needs metal/support cooperation.

References and Notes

(1) Chester, M. A.; McDougall, G. S.; Pemble, M. E.; Sheppard, N. *Surf. Sci.* **1985**, *164*, 425.

(2) Ortega, A.; Hoffman, F. M.; Bradshaw, A. M. *Surf. Sci.* **1982**, *119*, 79.

(3) Sheppard, N.; Nguyen, T. T. *Advanced in Infrared and Raman Spectroscopy*; Heyden: London, 1978; Vol. 5, pp 86–148.

(4) Henry, C. *Surf. Sci. Rep.* **1998**, *31*, 231.

(5) Goyhenex, C.; Croci, M.; Claeys, C.; Henry, C. R. *Surf. Sci.* **1996**, *352–354*, 475.

(6) Freund, H. J.; Bäumer, M.; Kuhlenbeck, H. *Adv. Catal.* **2000**, *45*, 333.

Surface Reactivity of Pd Nanoparticles

J. Phys. Chem. B, Vol. 108, No. 11, 2004 **3613**

(7) Jaeger, R. M.; Kuhlenbeck, H.; Freund, H.-J.; Wuttig, M.; Hoffmann, W.; Franchy, R.; Ibach, H. *Surf. Sci.* **1991**, *259*, 235.

(8) Libuda, J.; Winkelmann, F.; Bäumer, M.; Freund, H.-J.; Bertrams, T.; Neddermeyer, H.; Müller, K. *Surf. Sci.* **1994**, *318*, 61.

(9) Bäumer, M.; Freund, H.-J. *Prog. Surf. Sci.* **1999**, *61,* 127.

(10) Yudanov, I. V.; Sahnoun, R.; Neyman, K. M.; Rösch, N.; Hoffmann, J.; Schauermann, S.; Johánek, V.; Unterhalt, H.; Rupprechter, G.; Libuda, J.; Freund, H.-J. *J. Phys. Chem. B* **2003**, *107, 255.*

(11) Libuda, J.; Freund, H.-J. *J. Phys. Chem. B* **2002**, *106*, 4901.

(12) Schauermann, S.; Hoffmann, J.; Johánek, V.; Hartmann, J.; Libuda, J.; Freund, H.-J. *Angew. Chem., Int. Ed.* **2002**, *41*, 2532.

(13) Shaikhutdinov, S.; Heemeier, M.; Bäumer, M.; Lear, T.; Lennon, D.; Oldman, R. J.; Jackson, S. D.; Freund, H.-J. *J. Catal.* **2001**, *200*, 330.

(14) Rupprechter, G.; Unterhalt, H.; Morkel, M.; Galletto, P.; Hu, L.; Freund, H.-J. *Surf. Sci.* **2002**, *502–503,* 109.

(15) Somorjai, G. A. *Introduction to Surface Chemistry and Catalysis*; Wiley: New York, 1994.

(16) Sault, A. G.; Goodman, D. W. *Adv. Chem. Phys.* **1989**, *76*, 153.

(17) Xu, X.; Goodman, D. W. *J. Phys. Chem.* **1993**, *97*, 7711–7718.

(18) Somorjai, G. A.; Rupprechter, G. *J. Phys. Chem. B* **1999**, *103*, 162.

(19) Rupprechter, G.; Dellwig, T.; Unterhalt, H.; Freund, H.-J. *Top. Catal.* **2001**, *15*, 19.

(20) Goodman, D. W. *Surf. Sci.* **1994**, *299–300*, 837.

(21) Goodman, D. W. *Chem. Rev.* **1995**, *95*, 523.

(22) Rodriguez, J. A.; Goodman, D. W. *Surf. Sci. Rep.* **1991**, *14*, 1.

(23) Ertl, G.; Knözinger, H.; Weitkamp, J. *Handbook of Heterogeneous Catalysis*; Wiley-VCH: New York, 1997; Vol. 1–5. Cimino, A.; Stone, F. S. *Adv. Catal*. **2002**, *47*, 141.

(24) Zecchina, A.; Scarano, D.; Bordiga, S.; Spoto, G.; Lamberti, C. *Adv. Catal.* **2001**, *46*, 265–397.

(25) Bertarione, S.; Scarano, D.; Zecchina A.; Johánek, V.; Hoffmann, J.; Schauermann, S.; Libuda, J.; Rupprechter, G.; Freund, H.-J. *J. Catal*., in press.

(26) Libuda, J.; Meusel, I.; Hartmann, J.; Freund, H.-J. *Rev. Sci. Instrum.* **2000**, *71,* 4395.

(27) R Jaeger,. M.; Libuda, J.; Bäumer, M.; Homann, K.; Kuhlenbeck, H.; Freund, H.-J. *J. Electron Spectrosc. Relat. Phenom.* **1993**, *64/65*, 217.

(28) Meusel, I.; Hoffmann, J.; Hartmann, J.; Libuda, J.; Freund, H.-J. *J. Phys. Chem. B* **2001**, *105*, 3567.

(29) Meusel, I.; Hoffmann, J.; Hartmann, J.; Heemeier, M.; Bäumer, M.; Libuda, J.; Freund, H.-J. *Catal. Lett.* **2001**, *71*, 5.

(30) Shaikhutdinov, S.; Heemeier, M.; Hoffmann, J.; Meusel, I.; Richter, B.; Bäumer, M.; Kuhlenbeck, H.; Libuda, J.; Freund, H.-J.; Oldman, R. S.; Jackson, D.; Konvicka, C.; Schmid, M.; Varga, P. *Surf. Sci.* **2002**, *501,* 270.

(31) Libuda, J.; Meusel, I.; Hoffmann, J.; Hartmann, J.; Piccolo, L.; Henry, C. R.; Freund, H.-J. *J. Chem. Phys.* **2001**, *114,* 4669.

(32) Frank, M.; Bäumer, M. Private communication.

(33) Evans, J. V.; Whateley, T. L. *Trans. Faraday Soc.* **1967**, *63,* 2769.

(34) Matolin V.; Gillet, E. *Surf. Sci.* **1990**, *238,* 75–82.

(35) Giessel, T.; Schaff, O.; Hirschmugl, C. J.; Fernandez, V.; Schindler, K.-M.; Theobald, A.; Bao, S.; Lindsay, R.; Berndt, W.; Bradshaw, A. M.; Baddeley, C.; Lee, A. F.; Lambert, R. M.; Woodruff, D. P. *Surf. Sci.* **1998**, *406,* 90.

(36) Ortega, A. Ph.D. thesis, Technische Universität Berlin (Berlin), 1980.

(37) Tüshaus, M.; Berndt, W.; Conrad, H.; Bradshaw, A. M.; Persson, B. *Appl. Phys. A* **1990**, *51,* 91.

(38) Tüshaus, M. Ph.D. thesis, Freie Universität Berlin (Berlin), 1990.

(39) Loffreda, D.; Simon, D.; Sautet, P. *Surf. Sci.* **1999**, *425,* 68.

(40) Unterhalt, H.; Rupprechter, G.; Freund, H.-J. *J. Phys. Chem. B* **200**2, *106,* 356.

(41) Kuhn, W. K.; Szanyi, J.; Goodman, D. W. *Surf. Sci. Lett.* **1992**, *274,* L611.

(42) Wolter, K.; Seiferth, O.; Kuhlenbeck, H.; Bäumer, M.; Freund, H.-J. *Surf. Sci.* **1998**, *399,* 190.

(43) Frank, M.; Bäumer, M. *Phys. Chem. Chem. Phys.* **2000**, *2*, 3723.

(44) Hoffmann, F. M. *Surf. Sci. Rep.* **1983**, *3*, 107.

(45) Bäumer, M.; Libuda, J.; Freund, H.-J. In *Chemisorption and Reactivity on Supported Clusters and Thin Films*; Lambert, R. M., Pacchioni, G., Eds.; Kluwer Academic Press: Dordrecht, The Netherlands, 1997; p 61.

(46) Hollins, P. *Surf. Sci. Rep.* **1992**, *16*, 51.

(47) Schauermann, S.; Hoffmann, J.; Johánek, V.; Hartmann, J.; Libuda, J.; Freund, H.-J. *Catal. Lett.* **2002**, *84,* 209.

(48) Hansen, K. H.; Sljivancanin, Z.; Laegsgaard, E.; Besenbacher, F.; Stensgaard, I. *Surf. Sci.* **2002**, *505,* 25.

(49) Johanek, V.; Schauermann, S.; Laurin, M.; Libuda, J.; Freund, H.-J. *Angew. Chem., Int. Ed.*, in press.

(50) Yudanov, I. V.; Sahnoun, R.; Neyman, K. M.; Rösch, N. Manuscript in preparation.